Facile synthesis of indium doped CdSe thin films: microstructural and optoelectronic characteristics

G. T. Chavan[1,*] ![ORCID], S. T. Pawar[2], B. Y. Fugare[3], S. S. Kamble[4], P. C. Pingale[5],
Yedluri Anil Kumar[6], A. Sikora[7], Abdullah A. Al-Kahtani[8], and Chan-Wook Jeon[1,*]

[1] School of Chemical Engineering, Yeungnam University, Gyeongsan, Gyeongbuk 38541, Republic of Korea
[2] School of Physical Sciences, Punyashlok Ahilyadevi Holkar Solapur University, Solapur, Maharashtra 413255, India
[3] Jagdamb Mahavidyalaya, Achalpur, Amravati, Maharashtra 444806, India
[4] All India Council for Technical Education (AICTE), New Delhi 110070, India
[5] Department of Physics, T.C. College Baramati, Pune, Maharashtra 413102, India
[6] Department of Chemical and Petroleum Engineering, United Arab Emirates University, 15551 Al Ain, United Arab Emirates
[7] Department of Nanometrology, Faculty of Electronics, Photonics and Microsystems, Wroclaw University of Science and Technology, Janiszewskiego 11/17, 50-372 Wrocław, Poland
[8] Department of Chemistry, College of Science, King Saud University, P. O. Box 2455, Riyadh 11451, Saudi Arabia

ABSTRACT

Indium-doped CdSe has shown great potential as an active absorber and a window material in optoelectronic devices. In this communication, surface engineering of CdSe thin films was achieved by indium doping using an indigenously developed chemical growth technique. The substantial replacement of Cd^{2+} by In^{3+} was observed through the compositional studies. Surface microscopic studies revealed tiny spherical crystallites in a diffused environment with large inter-granular spacings. Atomic force microscopy shows an increased surface roughness and crystallite size. The energy band gap (E_g) of CdSe (1.80 eV) was shifted towards the ideal value (1.54 eV) with the integration of In^{3+} in the CdSe host. The In^{3+} impurity increases absorption, and upgrades the refractive index and dielectric constants (static, real, and imaginary) of CdSe thin films, further, beneficial to improve the performance of optoelectronic devices. The electrical conductivity was modulated up to 8.10×10^{-5} (Ω cm)$^{-1}$ for $x = 0.1$.

Address correspondence to E-mail: gtchavan1992@gmail.com; cwjeon@ynu.ac.kr

🍀 Springer

1 Introduction

The design and discovery of earth-abundant, versatile composite materials for energy conversion play a vibrant role in renewable energy solutions [1–5]. In the modern era, material industries and researchers across the globe concentrate on the improvement of novel next-generation/smart materials [6]. In this context, the II^A–VI^B chalcogenide semiconductor family gaining tremendous attention owing to their suitable material characteristics and practical applications [6–8]. Cadmium selenide (CdSe), an interesting photovoltaic semiconductor belongs to the II^A–VI^B group and has a direct bandgap of 1.7 eV, excellent luminous properties, with a high absorption coefficient, high electron affinity, and showing size quantization effect [9–11]. The intense research in the last five-six decades recognized CdSe as a multifunctional binary semiconductor, popular for a variety of outstanding technological/optoelectronic applications such as photodetectors, transistors, photoconductors, solar cells, lasers, sensors, LED, solar selective coatings, biomedical devices, and photoluminescent devices [9, 12–15]. Furthermore, the n-type CdSe material is a better substitute for expensive CdTe absorber material for solar cell application [16]. Whereas, Cd is toxic however Cd-based solar cells (CdSe and CdTe) have drawn the great consideration of researchers as possible substitutes for expensive Si-based solar cells and also for the less stable and quickly degradable perovskite solar cells [16]. However, reducing Cd use in the large-scale production of these CdSe and CdTe-based solar cells is necessary owing to toxicity and environmental threats [16, 17]. In this scenario, one way to accomplish this goal is to substitute the Cd from Cd-containing compounds while maintaining an improvement in efficiency [18].

The replacement of toxic Cd by intentional impurity addition in the CdSe compound acts as a chemical modifier that is greatly influential toward properties engineering of the semiconductors and thus offers unparalleled opportunities in the energy generation fields [5, 8, 13, 19]. The physical, structural, morphological, optical, and electrical transport properties could be tailored and developed employing doping/replacement of the host material with appropriate dopant atoms [5, 8, 13–17, 20]. Previously, pristine CdSe properties were modified by various dopants such as Mn, Ag, Al, B, Bi, Zn, Ga, Sb, Tl, Fe, Er, Ni, and In to meet the global demand for high-tech applications [20–22]. Among the various dopants, In has a similar ionic radius (0.94 Å) to Cd (0.97 Å) and consequently lower energy formation to replace the Cd [23, 24].

On the other hand indium selenide (InSe) belongs to the III-VI group metal–semiconductor and has fascinated tremendous attention owing to its high photo-response, tunable bandgap (1.4 to 2.6 eV), quantum confinement effect, phase-transition phenomena, high carrier mobility ($\sim 10^5$ cm^2 V^{-1} S^{-1}) and excellent electrical transport properties indicating a great potential in optoelectronic devices [18, 25, 27]. The phase diagram of InSe demonstrates that there are several stable phases with many stoichiometries such as InSe, In_2Se, In_3Se_2, In_4Se_3, In_5Se_6, In_6Se_7, In_3Se_4, In_2Se_3, and $In_{2.5}Se_4$, as observed in many reports [26]. Therefore, the substitutional replacement of Cd^{2+} by In^{3+} contributes free electrons, and enhance n-type characteristic resulting in decreased electrical resistivity [17, 28]. Till today different doping schemes such as intercalation, surface charge transfer, and substitution doping have been explored, among them substitution doping strategy was reported as the most stable way [25]. In this context, many researchers stated that the substitution of cadmium by indium was safe and capable of maintaining efficient PV performance [18]. Even though indium is an expensive element however, a small amount of indium doping was found to be suitable to modify and boost the different allied material properties for forthcoming absorber material applications [29]. Hence, indium has huge potential to modulate and engineer the materials features through the replacement of Cd is one of the prime objectives of our studies [8, 28]. Hence, we have decided to replace toxic Cd with non-toxic and stable In to form $In_xCd_{1-x}Se$ ternary compound by CBD method. Therefore, through this paper, we address the deposition of $In_xCd_{1-x}Se$ thin layers and their compositional, morphological characterizations, and thorough study of optoelectrical properties.

2 Methods and measurements

2.1 The materials synthesis

The deposition of $In_xCd_{1-x}Se$ ($0 \leq x \leq 0.1$) layers were carried out on micro-glass slide substrates (7.2 cm × 1 cm × 0.2 cm) in an alkaline chemical bath. Before deposition, the glass substrates were cleaned in an ultrasonic bath for 10 min by washing sequentially in ethanol, acetone, and double-distilled water (DDW), respectively. AR grade precursors [cadmium acetate, selenium metal powder, indium chloride sodium sulfite, ammonia, and tri-ethanolamine (TEA)] were used for the deposition of the $In_xCd_{1-x}Se$ compound. The Se-precursor (Na_2SeSO_3) was acquired by refluxing selenium metal powder with sodium sulfite at 80 °C for 9 h. The deposition of $In_xCd_{1-x}Se$ films was made feasible by mixing precursor solutions as; 10 ml (1 M) cadmium acetate, 2 ml triethanolamine (TEA), 15 ml aqueous ammonia, and 33 ml (0.33 M) sodium selenosulphate in a 100 ml glass beaker. An appropriate amount of $InCl_3$ was mixed in a reaction mixer to define the x value (In-content) from 0.025 to 0.1. The final reaction mixer's volume was made to 100 ml by the addition of DDW. The resulting pH was 10.1 ± 0.1. The reaction beaker containing precursors was shifted to a constant temperature paraffin oil bath (70 ± 0.1 °C). After 180 min the substrates were detached from the holder, washed with DDW, and desiccated carefully. The schematic of the actual chemical solution deposition method is given in Fig. 1.
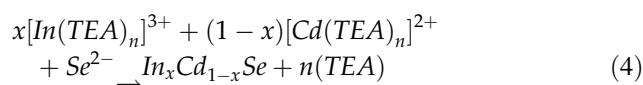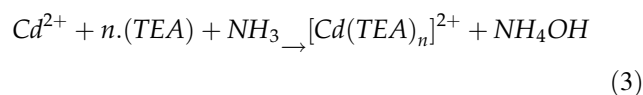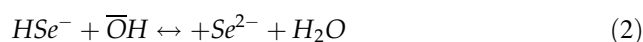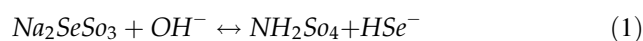
2.2 The characterization tools and techniques

The $In_xCd_{1-x}Se$ thin layers were characterized through the following techniques. The film thickness was determined by a Tencor P-16 + surface profilometer. The surface wettability test was performed by a computer-controlled goniometer by a Rame-Hart Inc. model-10 micro-syringe. Chemical composition and surface topography were then determined with an energy dispersive spectroscopy (EDS) unit connected to a scanning electron microscope (SEM) JEOL 6360-JED2300. High-angle annular dark-field (HAADF) scanning tunneling electron microscopy (STEM) was implemented for elemental mapping, and the surface nanostructures were inspected by

high-resolution transmission electron microscopy (TEM, Tecnai F21, FEI Company). The surface topographical insights were collected by an atomic force microscope (Innova, Bruker) in Tapping Mode at ambient conditions such as (k = 40 N/m, frequency = 290 kHz, and tip curvature < 10 nm). The data acquisition was done with the help of SPIP software from Image Metrology. The absorbance (αt) measurements, were done in the wavelength ranges from (400 nm to 1000 nm) using a BIO-AGE UV-Vis 2800 spectrophotometer. The electrical characteristics were measured by a two-probe technique in the temperature ranges from 350 to 550 K. The silver paste was applied to the well-defined area of the films to make good ohmic contacts. The voltage and current were recorded by the HIL 2665, $4_{1/2}$ digit multimeter, and DNM-121, $4_{1/2}$ digit nanoammeter, respectively. A chromel–alumel thermocouple was used to sense the working temperature.

3 Results and discussion

3.1 Reaction mechanism and physical observations

The principle of the chemical solution deposition method is to govern the chemical reaction to realize the deposition of a solid thin film by chemical precipitation [13]. The development of $In_xCd_{1-x}Se$ thin films relies on the discharge rate of Cd/In and Se ions and the development ensues with the sequential steps as follows [13];

$$Na_2SeSo_3 + OH^- \leftrightarrow NH_2So_4 + HSe^- \tag{1}$$

$$HSe^- + \overline{O}H \leftrightarrow +Se^{2-} + H_2O \tag{2}$$

$$Cd^{2+} + n.(TEA) + NH_3 \underset{\rightarrow}{} [Cd(TEA)_n]^{2+} + NH_4OH \tag{3}$$

$$x[In(TEA)_n]^{3+} + (1-x)[Cd(TEA)_n]^{2+} \\ + Se^{2-} \underset{\rightarrow}{} In_xCd_{1-x}Se + n(TEA) \tag{4}$$

As-deposited CdSe and $In_xCd_{1-x}Se$ films were relatively smooth, tightly adherent, and diffusely reflecting. The physical observations show film colour changes from an orange-red (CdSe) to faint orange-red as indium concentration increased from 0.025 to 0.1 as shown in Fig. 2 (Inset). When the x (In–content) changes from 0 to 0.1, the corresponding

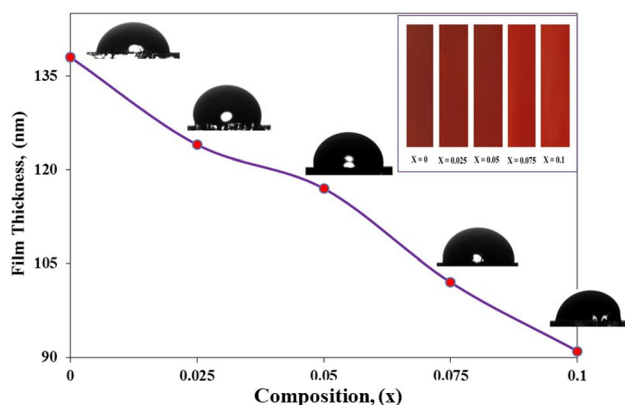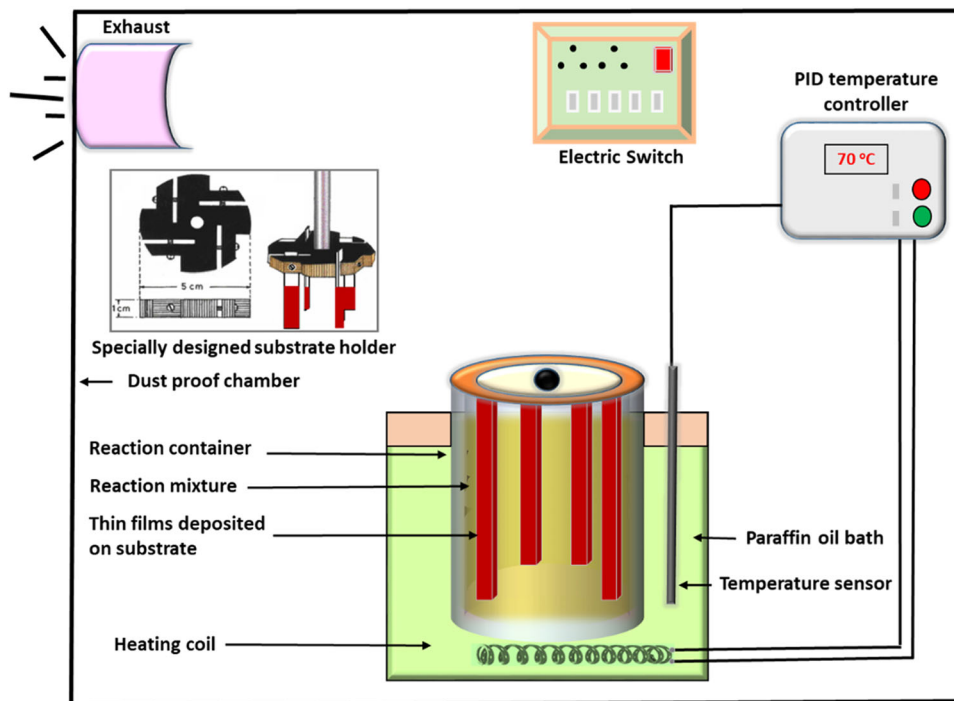**Fig. 1** Schematic of the chemical growth technique

Fig. 2 Film composition, (x) versus film thickness and contact angle (inset- colour indication of the materials)

film thickness was reduced from 138 to 91 nm (Fig. 2). With enhancing indium concentration in the CdSe host, the In ions can hold the interstitial sites of the CdSe lattice ensuing in a considerable impurity scattering and affecting a film thickness [1]. The surface wettability of as-deposited layers was studied to figure out the nature of the growth and the surface modifications in the films with x (Fig. 2). The pure CdSe, film growth is hydrophobic as $\theta > 90°$, whereas for In added samples, the contact angle decreased showing that the film tends to become hydrophilic (Table 1). Thus, $In_xCd_{1-x}Se$ thin films with a hydrophilic surface are useful as a window layer material and in electrochemical photovoltaic applications.

3.2 Compositional analysis

The atomic percentages of Cd, In, and Se in the as-deposited $In_xCd_{1-x}Se$ films are documented in Table 1. Our previous experimental reports indicated that the pristine CdSe is nearly stoichiometric [8, 13], while, the present case shows a slight deviation in stoichiometry (Cd/Se = 1.08). Pure CdSe samples are a little bit Cd-rich whereas, the addition of In in CdSe causes $In_xCd_{1-x}Se$ to be a bit Se-rich. The variation of Se-content in the films is not much significant. It should be noted that for film composition ranging from 0 to 0.075, Se^{2-} content in the film is nearly 50%. Thorough EDS analysis showed that In replaces Cd from the CdSe host with enhancing In-content. The atomic percentage of In is augmented continuously during the composition variation. This behaviour can be clarified as In^{3+} serving as a foreign inhomogeneity/nucleus which advances the growth mechanism [30]. The three representative EDS spectrographs for CdSe and $In_xCd_{1-x}Se$ samples are revealed in Fig. 3a–c.

Table 1 Some physical, compositional and microscopic measurements on CdSe and $In_xCd_{1-x}Se$ thin films

Composition (x)	Film thickness (nm)	Angle of contact (θ^0)	Atomic			In/Cd ratio (film)
			Cd	In	Se	
0	138	106	52.87	0	47.13	–
0.025	124	100	48.99	0.89	50.13	0.02
0.05	117	96	47.01	2.34	50.65	0.05
0.075	102	85	47.56	3.03	49.40	0.06
0.1	91	79	44.95	3.82	51.23	0.09
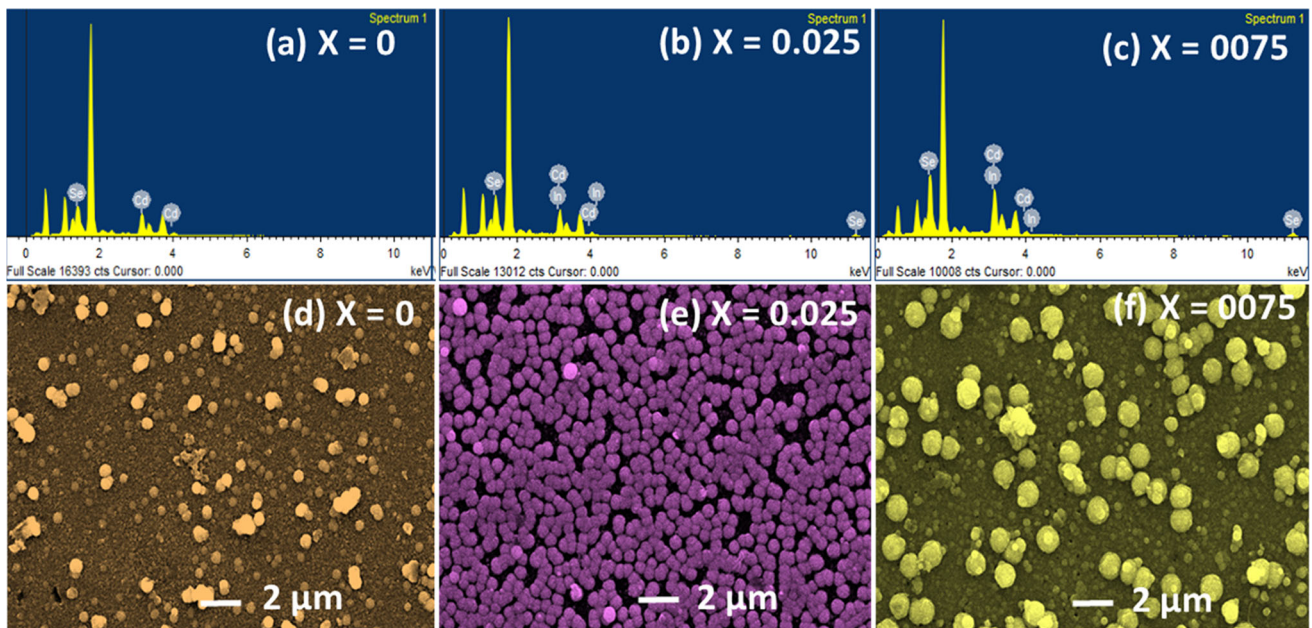
Fig. 3 **a–c** Typical three representative EDAX patterns and SEM micrographs of **d** $x = 0$, **e** $x = 0.025$, and **f** $x = 0.075$ for $In_xCd_{1-x}Se$ films

3.3 Morphological features

3.3.1 Scanning electron microscopy

Figure 3d–f shows SEM micrographs of the $In_xCd_{1-x}Se$ thin films. The CdSe films consist of spherical densely packed crystallites which are deeply embedded into an environment of smaller tiny crystallites. A sort of crystallite fusing has also been observed as bright spots in Fig. 3d. Previously, many authors observed the same kind of microstructure for CdSe thin films [13, 14]. The surface morphology of CdSe is improved significantly after In-doping. The grains retain their shape but the size is remarkably enhanced at the cost of inter-granular spacing (e.g. $x = 0.025$ and 0.05). The grains got well defined but a considerable increase in inter-granular spacing has been observed for higher In-concentration in CdSe (e.g. $x = 0.075$ and $x = 0.1$). At higher In-concentration, two or more grains initiate to form a globule-like growth. Thus, it is observed that the accumulation of In into the CdSe host, plays a key role in defining and crafting the surface properties like grain size distribution crystallinity and crystallite density, etc. The improved crystallinity with the increased size of spherical granules helps to improve light absorption and effectual spectral sensitivity which is beneficial in different optoelectronic applications.

3.3.2 Transmission electron microscopy (TEM)

The nanostructure of the CdSe ($x = 0$) and $In_xCd_{1-x}Se$ ($x = 0.075$) thin films was observed using TEM. Figure 4a, a_2, b, and b_2 shows different

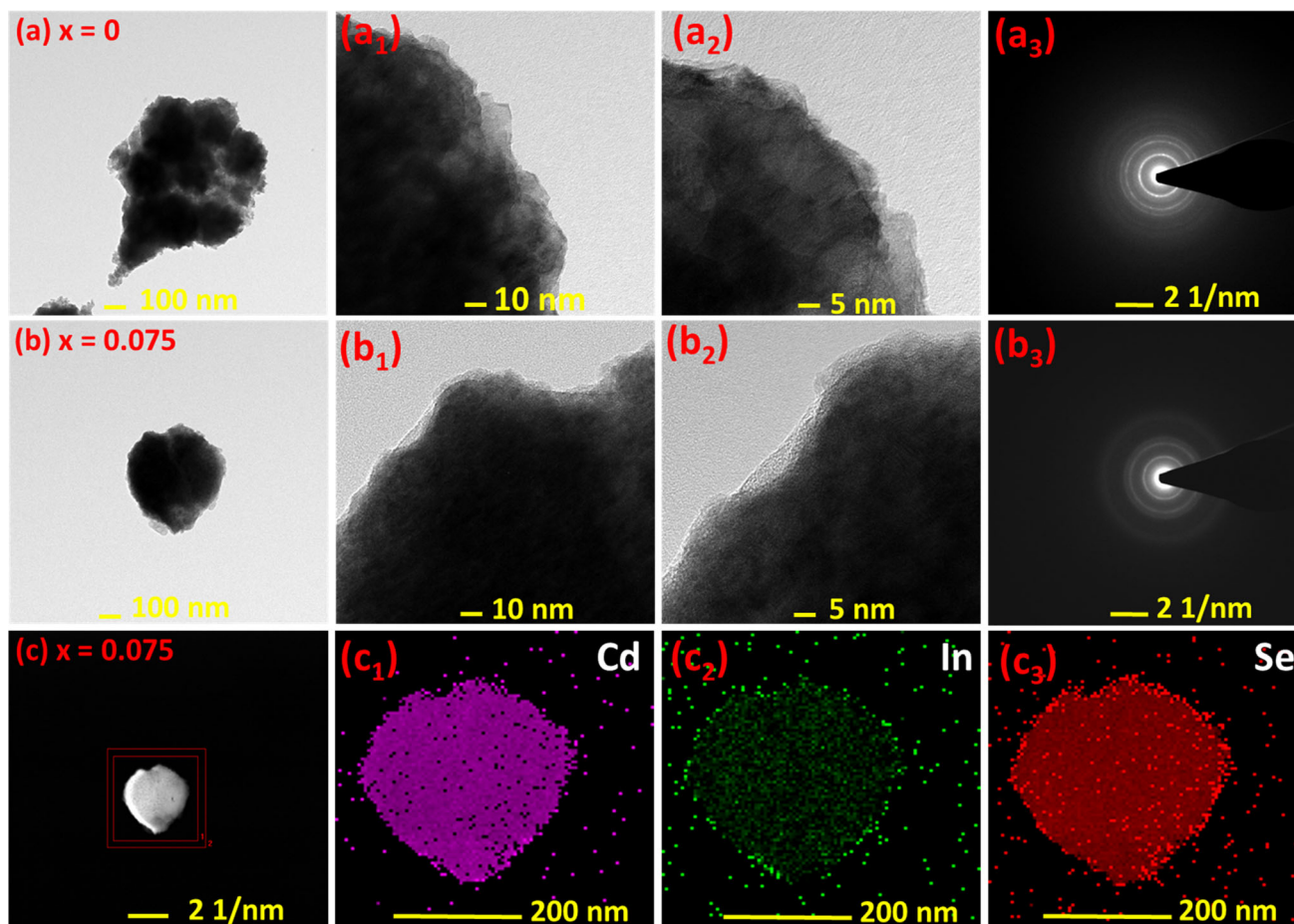**Fig. 4** **a**, **a₁**, **b**, **b₁** TEM and **a₂**, **b₂** HR-TEM images and **a₃**, **b₃** SAED pattern of the CdSe and $In_xCd_{1-x}Se$ films at $x = 0$ and 0.075, **c** selected region for EDS mapping of **c₁** Cd, **c₂** In and **c₃** Se elements and of the $In_xCd_{1-i}Se$ films at $x = 0.075$

magnification TEM images of $x = 0$, and $x = 0.075$ samples consisting of agglomerated spherical crystallites. A high-magnification TEM image (Fig. 4a2 and b2) displays the edges of CdSe and $In_xCd_{1-x}Se$ crystals. Figure 4a₃, b₃ reveals the selected area electron diffraction (SAED) pattern which suggests the crystalline nature of both CdSe and $In_xCd_{1-x}Se$ thin films. The EDAX elemental mapping and HAADF-STEM analysis of the $In_xCd_{1-x}Se$, ($x = 0.075$) sample revealed that the cadmium, indium, and selenide atoms are homogeneously distributed over the film surface, as displayed in Fig. 4c–c₃). Thus, TEM observations mimic our SEM observation and endorse the polycrystalline nature of the CdSe and $In_xCd_{1-x}Se$ thin films.

3.3.3 Atomic force microscopy

The 2D AFM topographs mimic the SEM micrographs as seen in Fig. 5a–c. The 3D AFM topographs

of as-grown $In_xCd_{1-x}Se$ films are shown in Fig. 5a₁–c₁. Surface topography of the CdSe and $In_xCd_{1-x}Se$ films showed the existence of hillocks and valleys, which is an indication of the crystalline nature of samples [1, 5]. With the addition of In the size of the hillocks enlarged and it seems that minor hillocks are merged into each other developing a large flat-topped hillock. Rather than sharp and well-defined crystalline hillocks, a considerable rounding of the hillocks was observed at higher doping levels (Fig. 5c1). The different AFM surface topographic parameters are cited in Table 2. For these samples, a higher value of RMS roughness was observed (Table 2). The positive skewness (S_{Sk}) moment for CdSe and $In_xCd_{1-x}Se$ suggests the surface has more hillocks than valleys. Hence In-doping causes, asymmetrical height distribution results in a more rough surface which may enhance light trapping and be useful for different optoelectronic device
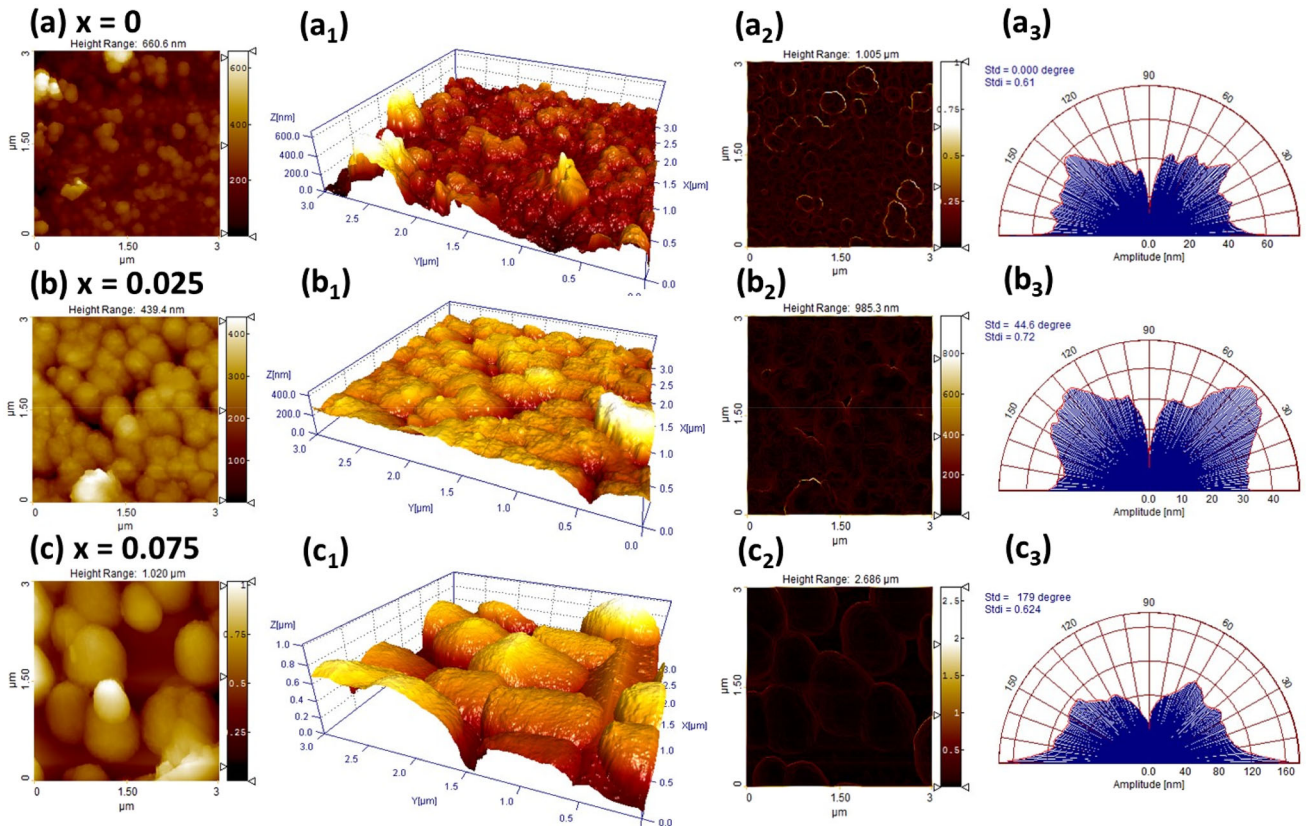
🌼 Springer

Fig. 5 **a–c** 2D, **a$_1$–c$_1$** 3D-AFM topographs of CdSe and In$_x$Cd$_{1-x}$Se thin films **a$_2$–c$_2$** Sobel transformation and **a$_3$–c$_3$** angular spectra for same films

Table 2 AFM studies on CdSe and In$_x$Cd$_{1-x}$Se thin films

Composition (x)	Avg. roughness S_a (nm)	RMS roughness S_q (nm)	Avg. max. profile peak height, S_{pk} (nm)	Avg. max. profile valley depth S_{vk} (nm)	Skewness S_{sk}	Kurtosis moment S_{ku}	Surface area ratio S_{dr} (%)
0	235.75	250.10	69.71	93.79	1.115	1.304	112.42
0.025	244.17	260.18	127.26	29.51	1.310	1.987	104.80
0.05	332.00	344.26	63.28	100.75	1.093	1.244	71.70
0.075	392.40	418.74	139.69	177.37	1.119	1.321	117.43
0.1	316.08	350.77	89.22	121.53	1.128	1.345	71.41

applications [31]. The irregularity in the height distribution of the AFM topography was studied through the Kurtosis measurements. When $S_{ku} = 3$, the surface is mesokurtic, while if ($S_{ku} < 3$), the surface becomes platykurtic (spiky surfaces), if the $S_{ku-} > 3$, then called leptokurtic (bumpy surfaces) [1, 5]. Pristine CdSe and In$_x$Cd$_{1-x}$Se films having ($S_{ku} < 3$) signpost growth of the samples was platykurtic nature (domination of hillocks over valleys is confirmed). It has also been reported that to boost the

efficiency of PV-device, rough topography of the absorber materials is required; the rougher surfaces have the advantage of enhancing the contact area of the active layer with the top contact layer which can enhance the short circuit current density remarkably [31]. The Sobel transformation, an advanced imaging technique was also used for edge detection of topography and better visibility of grains [5] which highlighted the agglomeration of spherical and flat-topped larger grains (Fig. 5a2–c2). Angular spectra

studies designated the presence of a privileged orientation of the morphological features (Fig. 5a3–c3).

3.4 Optical studies

The optical absorbance (αt) of the CdSe and In_x-Cd_{1-x}Se films was measured from the 400 nm to 1200 nm wavelength range. The absorption coefficient (α) was evaluated and was found to be high as expected ($\alpha \approx 10^4$ cm^{-1}) [13, 14]. The variation of an absorption coefficient (α) vs λ is shown in Fig. 6a. Tauc's plots are mainly used to determine the band gaps (E_g) of semiconductor thin films and to assess the influence of doping on the optical characteristics of the material.

The Tauc's relation was used to determine the bandgap [13, 32];

$$\alpha h\upsilon = A(h\upsilon - Eg)^m, \tag{5}$$

where α is the absorption coefficient, A is a constant,

and $h\upsilon$ is the energy of a photon. The energy E_g values are determined from $(\alpha h\upsilon)^2$ versus $h\upsilon$ graphs (Fig. 6b) [13, 32]. From Table 3 the E_g of pure CdSe is found to be 1.80 eV and was decreased upto 1.54 eV for $x = 0.1$. This decrement in E_g can be credited to the development of additional donor states in the bandgap by the addition of In into the CdSe host matrix. However, the reduction in the E_g towards the maxima of the solar spectrum is advantageous for the fabrication of window materials in solar cells [33]. The extinction coefficient (k) is the amount of light absorbed or/and scattered as light pass through the material. The k was calculated from the relation [32, 33].

$$k = \alpha\lambda/4\pi, \tag{6}$$

where α is the absorption coefficient, and λ is the wavelength. From Table 3 it is observed that the k value increases with In composition. The higher value of k for In_xCd_{1-x}Se samples indicates

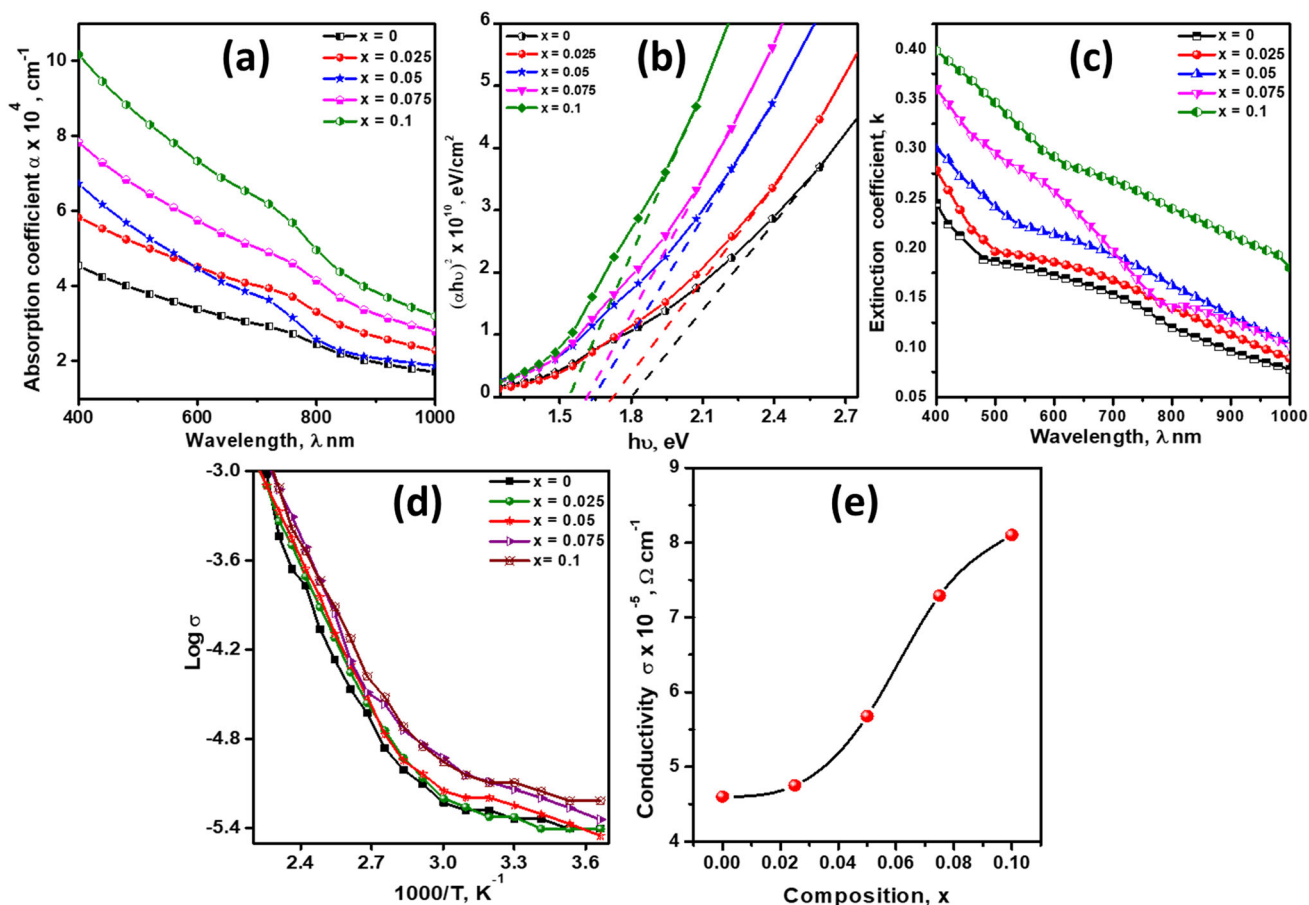**Fig. 6** Plots of **a** absorption coefficient (α) vs wavelength (λ), **b** determination of optical band gap, **c** dependence of the extinction coefficient (k) upon the wavelength photons **d** Log σ vs 1000/T, and **e** electrical conductivity vs film composition

Table 3 Optical parameters of CdSe, and $In_xCd_{1-x}Se$ thin films

Composition (x)	Band gap (E_g) eV	Extinction coefficient (k)	Real dielectric constant (ε_1)	Imaginary dielectric constant (ε_2)	Static dielectric constant (ε_0)	High frequency dielectric constant (ε_∞)	Electrical conductivity ($\sigma \times 10^{-5}$) $(\Omega\,cm)^{-1}$
0	1.80	0.167	6.746	0.878	6.916	8.698	4.60
0.025	1.72	0.182	7.218	0.979	7.236	9.091	4.75
0.05	1.64	0.214	7.601	1.181	7.617	9.447	5.68
0.075	1.61	0.255	7.771	1.422	7.784	9.567	7.29
0.1	1.54	0.290	8.113	1.653	8.122	9.805	8.10

absorption per unit distance was high and less energy was lost by scattering when light passes through $In_xCd_{1-x}Se$ films [35]. At the higher wavelength side (> 800 nm) the k values are in the range of 0.01 or less, which denotes slite or irrelevant dissipation of energy, of the propagated electromagnetic waves (EM), by the scattering or absorption. Figure 6c reveals k-values are suddenly dropping and reaching zero at a higher wavelength range. This decrement of the k-value with increasing wavelength specifies that as-deposited thin films permit EM to propagate without any loss or damping in the NIR-spectral region. This behaviour of k demonstrates $In_xCd_{1-x}Se$ films become good absorber material [35, 36]. Hassanien et al. and others have found similar behaviour of k for several semiconducting materials [35–37]. The knowledge about the dielectric constant of material was beneficial for the design and development of different next-generation charge storage devices, microwave devices, etc. [38].

The real and imaginary dielectric constants (ε_1) and (ε_2) are determined by the following equations [32, 34].

$$\varepsilon_1 = n^2 - k^2 \tag{7}$$

The real dielectric constant accounts for energy stored in the material and influences the electromagnetic wave (EM) dispersion which further origins a reduction in the velocity of incident photons while propagating in a medium (film) [34, 37].

$$\varepsilon_2 = 2nk \tag{8}$$

However, the ε_2 signifies the polarization losses in the film. On the other hand, ε_2 illustrates the dissipation or energy loss within the medium [34]. The imaginary part of the dielectric constant is very less as compared to the real part. Table 3 depicts both the

(ε_1) and (ε_2) values increased with In-content. The increment of ε_1 suggests that In enhances the dispersion and therefore, indium was responsible for decreasing the speed of the propagated EM. Similarly, enhancement in (ε_2) by integration of In, also states about augmentation of the energy loss within the film [34]. The simultaneous integration of S and Se in CdSe showed a similar trend for ε_1 and ε_2 [32], and in the present case, ε_1 and ε_2 exhibit the same behaviour as that of k.

The high-frequency dielectric constant (ε_∞) is determined by the following equation [32]

$$\varepsilon_\infty = n^2 \tag{9}$$

Table 3 displays that the values of (ε_∞) are higher than the index of refraction. This behaviour of (ε_∞) designates the existence of the free charge carriers in the $In_xCd_{1-x}Se$ films [37].

The static dielectric constant (ε_o) is determined by the following equation [32];

$$\varepsilon_0 = 33.26876 + 78.61805E_g - 45.70795E_g{}^2 + 8.32449E_g{}^3 \tag{10}$$

The static dielectric constant (ε_0) follows the same trend as n, k, ε_1, and ε_2.

3.5 Electrical transport studies

Figure 6 e reveals the Arrhenous behaviour with the semiconducting nature of the CdSe and $In_xCd_{1-x}Se$ films. In the conductivity plot the low-temperature range (300 K to 360 K) is associated with intrinsic conduction (variable range hopping) and the high-temperature region (360 K to 550 K)is related to extrinsic conduction (grain boundary scattering limited conduction mechanism) [8, 15]. The conductivity of the pristine CdSe was found to be 4.60×10^{-5}

⚛ Springer

$(\Omega \, cm)^{-1}$ which is in good consonance with recently stated values [8, 13]. The electrical conductivity (σ) was found to be improved continuously with an increase in x (Table 3). The highest electrical conductivity of 8.10×10^{-5} $(\Omega \, cm)^{-1}$ was observed at $x = 0.1$ shown in Fig. 6e. Thus, the substitution of a Cd by In is more advantageous which causes the boosting of electrical conductivity [11]. The increase in electrical conductivity can be credited to the reduced energy gap and improvement in the grain structure as a result of In corroboration in the CdSe matrix. Our previous attempt of substitutional Al^{3+} doping in the CdSe host exhibited similar electrical conductivity outcomes to $In_xCd_{1-x}Se$ [14].

4   Conclusion

The deposition of ternary $In_xCd_{1-x}Se$ films was made feasible using an inexpensive chemical deposition technique. The compositional analysis exhibited the formation of the ternary $In_xCd_{1-x}Se$ films. The surface morphology showed swollen spherical crystallites with varying inter-crystalline spacings on In-integration. AFM results presented domination of hillocks over valleys and the growth of the samples was platykurtic. Optical studies revealed a high absorption coefficient of $\sim 10^{-4} \, cm^{-1}$ and E_g is shifted towards the ideal value (1.54 eV for $x = 0.1$). Integration of In increases extinction coefficient (k) values. The deviation of dielectric constants (real and imaginary) with photon energy suggests the interaction between the incident photons and free electrons. Electrical transport studies showed conductivity modulation by In-integration. Finally, our finding reveals doping of indium improves the morphology and optoelectronic properties of the CdSe films. Therefore, a comprehensive study of the $In_xCd_{1-x}Se$ films deposited by a facile and inexpensive chemical deposition process can offer a valuable addition to the field of optoelectronics, and such types of doped chalcogenides can be employed in various optoelectronic applications.

Author contribution

G.T. Chavan: Writing–Conceptualization, Original Draft. S.T. Pawar–Data Curation, B.Y. Fugare–

Software. S.S. Kamble—Writing-Review and Editing. P.C. Pingale–Formal analysis. Yedluri Anil Kumar–Writing-Review, Resources, Investigation, Validation. A. Sikora–Visualization, Validation. Abduallah A AlKahtani—Writing-Review, Funding acquisition, Supervision. Chan-Wook Jeon–Project administration, Funding acquisition.

Data availability

The data will be made available on resonable request.

Declarations

Competing interest   The authors declare that they have no known competing financial interests or personal relationships that could have appeared to influence the work reported in this paper.

References

1. G.T. Chavan, F.A. Sabah, S.S. Kamble, V.M. Prakshale, S.T. Pawar, S. Patil, S. Lee, A. Sikora, L.P. Deshmukh, Y. Cho, E.C. Cho, J. Yi, Novel synthesis method for quaternary Cd(Cu, Zn)Se thin films and its characterizations. Ceram. Int. **46**, 74–80 (2020)
2. Y. Lu, Y. Jiang, Z. Lou, R. Shi, D. Chen, G. Shen, Wearable supercapacitor self- charged by P(VDF-TrFE) piezoelectric separator. Prog. Nat. Sci. Mater. Int. **30**, 174–179 (2020)
3. S. Zheng, J. Ma, K. Fang, S. Li, J. Qin, Y. Li, J. Wang, L. Zhang, F. Zhou, F. Liu, K. Wang, Z.S. Wu, High-voltage potassium ion micro-supercapacitors with extraordinary volumetric energy density for wearable pressure sensor system. Adv. Energy Mater. **11**, 2003835 (2021)

Ⓐ Springer

4. Z. Wu, X. Yang, H. Gao, H. Shen, H. Wu, X. Xia, X. Wu, W. Lei, J. Yang, Q. Hao, Controllable synthesis of $ZnCo_2O_4@$-$NiCo_2O_4$ heterostructures on Ni foam for hybrid supercapacitors with superior performance. J. Alloys Compd. **891**, 162053 (2021)

5. G.T. Chavan, N.M. Shinde, F.A. Sabah, S.S. Patil, A. Sikora, V.M. Prakshale, S.S. Kamble, N.B. Chaure, L.P. Deshmukh, A. Kim, C.W. Jeon, Chemical synthesis of $Cd_{1-x-y}Zn_xCu_yS_{z-}Se_{1-z}$ composite thin films for photoelectrochemical solar cell. Appl. Surf. Sci. **574**, 151581 (2022)

6. I. Sharma, A.S. Hassanien, Effect of Ge-addition on physical and optical properties of chalcogenide $Pb_{10}Se_{90-x}Ge_x$ bulk glasses and thin films. J Non Cryst Solids **548**, 120326 (2020)

7. A. Kathalingam, S. Valanarasu, T. Ahamad, S.M. Alshehri, H.S. Kim, Spray pressure variation effect on the properties of CdS thin films for photodetector applications. Ceram. Int. **47**, 7608–7616 (2021)

8. G.T. Chavan, S.T. Pawar, V.M. Prakshale, S.M. Pawar, S. Ezugwu, N.B. Chaure, S.S. Kamble, N.N. Maldar, L.P. Deshmukh, Direct synthesis of quaternary Cd(Zn, S)Se thin films: effects of composition. Mater. Sci. Semicond. Proces. **71**, 447–453 (2017)

9. T.C.M. Santhosh, K.V. Bangera, G.K. Shivakumar, Effect of Bi doping on the properties of CdSe thin films for optoelectronic device applications. Mater. Sci. Semicond. Process. **68**, 114 (2017)

10. G. Degdas, A. Peksoz, Electrodeposition of in: CdSe precursor thin films in aqueous electrolytes including different selenous acid concentrations as Se source. Mater. Sci. Semicond. Process. **104**, 104655 (2019)

11. V.S. Raut, C.D. Lokhande, H.D. Shelke, V.V. Killedar, Studies on modulated physical and photoelectrochemical properties of CdSe thin films by means of Indium doping. J Mater Sci: Mater Electron. **33**, 13782–13791 (2022)

12. K. Sharma, A.S. Al-Kabbi, G.S.S. Saini, S.K. Tripathi, Indium doping induced modification of the structural, optical and electrical properties of nanocrystalline CdSe thin films. J. Alloys Compd. **564**, 42–48 (2013)

13. G.T. Chavan, S.S. Kamble, N.B. Chaure, N.N. Maldar, L.P. Deshmukh, Invoking stoichiometric protocols for chemical synthesis of CdSe thin films. J. Alloys Compd. **680**, 139–145 (2016)

14. G.T. Chavan, A. Sikora, N.B. Chaure, L.P. Deshmukh, J. Chan-Wook, A novel highly conductive chalcogenide material: $Cd_{1-x}Al_xSe$ thin films. Mater. Lett. **320**, 132353 (2022)

15. G.T. Chavan, V.M. Prakshale, S.T. Pawar, P.R. Deshmukh, A. Sikora, S.S. Kamble, N.N. Maldar, L.P. Deshmukh, Morphology improvements in CdSe thin films: a realization through mechanical agitation and incubation period. Nano-Struct. Nano-Objects **12**, 113–120 (2017)

16. G. Himanshu, D. Chasta, A. Suthar, M.D. Thakur, M.S. Kannan, Dhaka, Comprehensive investigation on influence of copper doping on physical properties of CdSe thin films for solar cell applications. Mater. Res. Bull. **152**, 111845 (2022)

17. S. Butt, N.A. Shah, A. Nazir, Z. Ali, A. Maqsood, Influence of film thickness and In-doping on physical properties of CdS thin films. J. Alloys Compd. **587**, 582–587 (2014)

18. A. Timoumi, W. Belhadj, S.N. Alamri, M.K. Al Turkestani, Experimental studies and new theoretical modeling on the properties of In_2S_3 thin films. Opt. Mater. **118**, 11123 (2021)

19. S.T. Pawar, G.T. Chavan, V.M. Prakshale, A. Sikora, S.M. Pawar, S.S. Kamble, N.N. Maldar, L.P. Deshmukh, Physical, structural and topographical aspects of $Zn_{1-x}Co_xSe$ thin films. Mater Sci Semicond Process. **61**, 71–78 (2017)

20. F.J. Willars-Rodríguez, I.R. Chavez-Urbiola, R. Ramírez-Bon, P. Vorobiev, Y.V. Vorobiev, Effects of aluminum doping in CdS thin films prepared by CBD and the performance on Schottky diodes TCO/CdS:Al/C. J. Alloys Compd. **817**, 152740 (2020)

21. G. Degdas, A. Peksoz, Electrodeposition of in: CdSe precursor thin films in aqueous electrolytes including different selenous acid concentrations as Se source. Mater. Sci. Semicond. Proces. **104**, 104655 (2019)

22. I.R. Chavez-Urbiola, M.I. Pintor-Monroy, F.J. Willars-Rodriguez, Y.V. Vorobiev, R. Ramírez-Bon, M.A. Quevedo-Lopéz, Effects of aluminum doping upon properties of cadmium sulfide thin films and its effect on ITO/CdS:Al/NiO_x/Ni/Au diodes. J. Appl. Phys. **126**, 115702 (2019)

23. T.M. Cheng, C.H. Cai, W.C. Huang, W. Xu, L.H. Tu, C.H. Lai, Efficiency enhancement of Cu(In, Ga)(S, S_e)2 solar cells by indium doped CdS buffer layers. ACS Appl. Mater. Interfaces **12**, 18157–18164 (2020)

24. C. Tuinenga, J. Jasinski, T. Iwamoto, V. Chikan, In situ observation of heterogeneous growth of CdSe quantum dots: effect of indium doping on the growth kinetics. ACS Nano **2**, 1411–1421 (2008)

25. C. Zhang, X. Chen, B. Cao, H. Duan, Q. Sun, F. Ouyang, Tuning the band gap of the InSe monolayer by substitutional doping. Appl. Surf. Sci. **579**, 15 (2022)

26. B.K. Mondal, S.K. Mostaque, Md.A. Islam, J. Hossain, Stress-induced phase-alteration in solution processed indium selenide thin films during annealing. RSC Adv. **11**, 13751–13762 (2021)

27. Y. Bchiri, B. Tiss, N. Bouguila, R. Souissi, M. Kraini, C. Vazquez-Vazquez, K. Khirouni, S. Alaya, Electrical investigation of sprayed In_2S_3 film. Mater Sci Semicond Process. **121**, 105294 (2021)

28. C. Wu, C. Jiang, X. Wang, H. Ding, H. Ju, L. Zhang, T. Chen, C. Zhu, Interfacial engineering by indium-doped CdS for high

efficiency solution processed $Sb_2(S_{1-x}Se_x)_3$ Solar Cells. ACS Appl. Mater. Interfaces **11**, 3207–3213 (2019)

29. M. Shkir, M. Anis, S.S. Shaikh, S. AlFaify, An investigation on structural, morphological, optical and third order nonlinear properties of facilely spray pyrolysis fabricated in: CdS thin films. Superlattices Microstruct. **133**, 106202 (2019)

30. G.T. Chavan, A. Yadav, B.Y. Fugare, N.M. Shinde, M.S. Tamboli, S.S. Kamble, A. Sikora, J. Warycha, B.J. Lokhande, S.W. Kang, A. Kim, C.W. Jeon, Three dimensional hierarchical flower-like $CoCuS/Co_{1-x}Cu_xS$ electrodes for electrochemical supercapacitors. J. Alloys Compd. **901**, 162822 (2022)

31. T. Sharma, R. Singhal, R. Vishnoi, P. Sharma, A. Patra, S. Chand, G.B.V.S. Lakshmi, S.K. Biswas, Electronic excitation induced modifications of optical and morphological properties of PCBM thin films. Nucl. Instrum. Methods Phys. Res. B: Beam Interact Mater. At. B **379**, 176–180 (2016)

32. G.T. Chavan, V.M. Prakshale, S.S. Kamble, S.T. Pawar, A. Sikora, E.C. Cho, J. Yi, L.P. Deshmukh, Cd (Zn, S) Se quaternary thin films for electrochemical photovoltaic cell application. Int. J. Energy Res. **44**, 3737–4374 (2020)

33. A.A. Yadav, Influence of film thickness on structural, optical, and electrical properties of spray deposited antimony doped SnO_2 thin films. Thin Solid Films **591**, 18–24 (2015)

34. A.S. Hassanien, I.M. El Radaf, Optical characterizations of quaternary Cu_2MnSnS_4 thin films: novel synthesis process of film samples by spray pyrolysis technique. Phys. B: Condens. Matter. **585**, 412110 (2020)

35. A.S. Hassanien, Studies on dielectric properties, opto-electrical parameters and electronic polarizability of thermally evaporated amorphous $Cd_{50}S_{50-x}Se_x$ thin films. J. Alloys Compd. **671**, 566–578 (2016)

36. A.S. Hassaniena, R. Neffatic, K.A. Aly, Impact of Cd-addition upon optical properties and dispersion parameters of thermally evaporated $Cd_xZn_{1-x}Se$ films: discussions on bandgap engineering, conduction and valence band positions. Optik (Stuttg.) **212**, 164681 (2020)

37. A.S. Hassanien, I. Sharma, Optical properties of quaternary a-$Ge_{15-x}Sb_xSe_{50}Te_{35}$ thermally evaporated thin-films: refractive index dispersion and single oscillator parameters. Optik (Stuttg.) **200**, 163415 (2020)

38. S.T. Pawar, G.T. Chavan, V.M. Prakshale, S.R. Jadkar, S.S. Kamble, N.N. Maldar, L.P. Deshmukh, Probing into the optical and electrical properties of hybrid $Zn_{1-x}Co_xSe$ thin films. J. Mater. Sci.: Mater. Electron **29**, 3704–3714 (2018)

Terms and Conditions

Springer Nature journal content, brought to you courtesy of Springer Nature Customer Service Center GmbH ("Springer Nature").

Springer Nature supports a reasonable amount of sharing of research papers by authors, subscribers and authorised users ("Users"), for small-scale personal, non-commercial use provided that all copyright, trade and service marks and other proprietary notices are maintained. By accessing, sharing, receiving or otherwise using the Springer Nature journal content you agree to these terms of use ("Terms"). For these purposes, Springer Nature considers academic use (by researchers and students) to be non-commercial.

These Terms are supplementary and will apply in addition to any applicable website terms and conditions, a relevant site licence or a personal subscription. These Terms will prevail over any conflict or ambiguity with regards to the relevant terms, a site licence or a personal subscription (to the extent of the conflict or ambiguity only). For Creative Commons-licensed articles, the terms of the Creative Commons license used will apply.

We collect and use personal data to provide access to the Springer Nature journal content. We may also use these personal data internally within ResearchGate and Springer Nature and as agreed share it, in an anonymised way, for purposes of tracking, analysis and reporting. We will not otherwise disclose your personal data outside the ResearchGate or the Springer Nature group of companies unless we have your permission as detailed in the Privacy Policy.

While Users may use the Springer Nature journal content for small scale, personal non-commercial use, it is important to note that Users may not:

1. use such content for the purpose of providing other users with access on a regular or large scale basis or as a means to circumvent access control;

2. use such content where to do so would be considered a criminal or statutory offence in any jurisdiction, or gives rise to civil liability, or is otherwise unlawful;

3. falsely or misleadingly imply or suggest endorsement, approval , sponsorship, or association unless explicitly agreed to by Springer Nature in writing;

4. use bots or other automated methods to access the content or redirect messages

5. override any security feature or exclusionary protocol; or

6. share the content in order to create substitute for Springer Nature products or services or a systematic database of Springer Nature journal content.

In line with the restriction against commercial use, Springer Nature does not permit the creation of a product or service that creates revenue, royalties, rent or income from our content or its inclusion as part of a paid for service or for other commercial gain. Springer Nature journal content cannot be used for inter-library loans and librarians may not upload Springer Nature journal content on a large scale into their, or any other, institutional repository.

These terms of use are reviewed regularly and may be amended at any time. Springer Nature is not obligated to publish any information or content on this website and may remove it or features or functionality at our sole discretion, at any time with or without notice. Springer Nature may revoke this licence to you at any time and remove access to any copies of the Springer Nature journal content which have been saved.

To the fullest extent permitted by law, Springer Nature makes no warranties, representations or guarantees to Users, either express or implied with respect to the Springer nature journal content and all parties disclaim and waive any implied warranties or warranties imposed by law, including merchantability or fitness for any particular purpose.

Please note that these rights do not automatically extend to content, data or other material published by Springer Nature that may be licensed from third parties.

If you would like to use or distribute our Springer Nature journal content to a wider audience or on a regular basis or in any other manner not expressly permitted by these Terms, please contact Springer Nature at

onlineservice@springernature.com